Supporting Information

1. Characterization of the coating feed solution and the spray coating

1.1 Solution viscosity

Viscosity was measured using a rotational viscometer under controlled room temperature conditions (25 °C). For each coating formulation, the viscosity was determined prior to spraying to assess its flow behavior and suitability for atomization. Each sample was measured three times, and the mean value was calculated. The unit of viscosity is expressed in millipascal-seconds (mPa·s).

1.2 Transmittance measurement

The light transmittance of the edible film was determined by testing its solution before spraying using a UV-visible spectrophotometer at 660 nm (Singh et al., 2015). According to Beer-Lambert Law, the transmittance T (%) is calculated as: T=10^−A×100, where T：transmittance (Expressed as a percentage %), A: Absorbance (Abs).

1.3 Moisture content (MC)

The moisture content (MC) of the edible films was determined by gravimetric analysis. Each film sample was first weighed to record the initial mass (W_1) and then dried in a hot air oven at 105 °C for 8 hours. After drying, the samples were cooled in a desiccator to room temperature and reweighed to obtain the final dry mass (W_2). The moisture content was calculated using the following equation:

$$MC(\%) = \frac{w_1 - w_2}{w_1} \times 100$$

Here, W_1 represents the initial mass of the film sample before drying, and W_2 denotes the final dry mass of the film sample after drying. To ensure the reliability and reproducibility of the results, each measurement was conducted in triplicate. The moisture content values were reported as the mean ± standard deviation of these replicates, providing clear insights into the consistency and reliability of the experimental outcomes.

1.4 Water solubility (WS)

Pre-dried film samples were immersed in distilled water at room temperature (~25 °C) for 24 hours. After immersion, the samples were carefully removed, and excess surface water was gently blotted with filter paper. The remaining film residue was then dried at 105 °C for 8 hours, cooled in a desiccator, and weighed to record the final dry mass (DM_2). The initial dry mass before immersion (DM_1) was obtained from the pre-dried films.The water solubility was calculated using the following equation:

where DM_1 is the initial dry mass before immersion, and DM_2 is the final dry mass after immersion and drying. Each test was conducted in triplicate, and values were expressed as mean ± standard deviation.

$$MS(\%) = \frac{DM_1 - DM_2}{DM_1} \times 100$$

where DM_1 (g) is the initial dry mass before immersion, and DM_2 (g) is the final dry mass after immersion and drying. Each test was conducted in triplicate, and values were expressed as mean ± standard deviation.

2. Supplementary results

2.1 Optimizing spraying conditions

The spray distance affects the particle flight time in the jet, thereby determining their temperature and velocity upon impact with the substrate, which significantly influences the coating formation process (Ren et al., 2023). In this study, the spraying distance was set at 15 cm and the spraying time was 10 seconds. These parameters were determined based on the previous experiments, aiming to achieve a uniform and continuous coating while avoiding excessive material loss or spraying spatter. A spraying distance of 15 cm achieves a good balance between droplet diffusion and deposition efficiency, ensuring that the coating solution can fully adhere to the substrate while avoiding sputtering or premature drying of droplets before contact. And the differences between the 5 cm, 10 cm samples and 15 cm samples can be seen from Fig. S1. At both 5 cm and 10 cm spraying distances, the coating solution exhibited significant displacement due to excessive airflow force, leading to non-uniform film formation and surface irregularities. A 10-second spraying time is considered sufficient to form a consistent coating on the target surface, achieving uniform coverage without causing overly thick film layers or material accumulation. Therefore, these two parameters were determined as the standard spraying conditions in this study to ensure good repeatability and consistency among all samples.

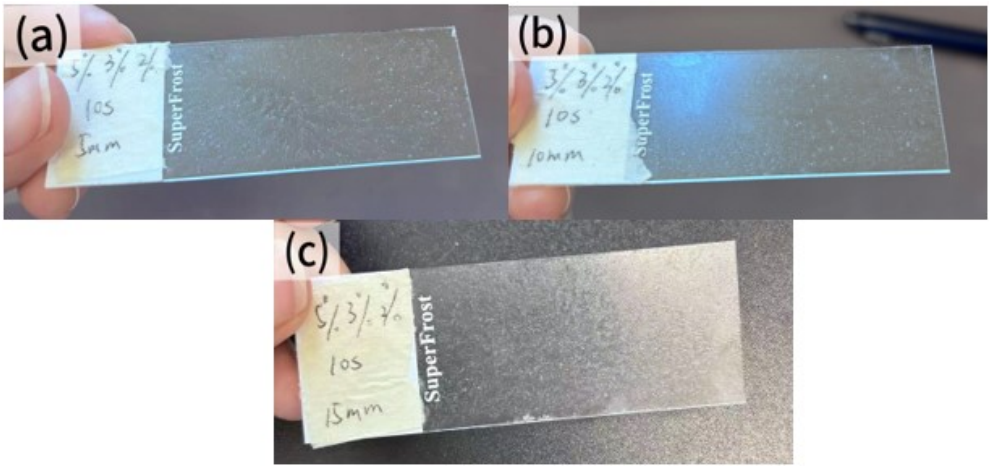

Fig. S1 Visual comparison of film morphology for a constant coating formulation sprayed at varying distances: (a) 5 cm, (b) 10 cm, (c) 15 cm. Influence of nozzle-to-substrate gap on surface uniformity and coverage.

2.2 Viscosity analysis

Viscosity is one of the key parameters affecting the rheological behavior and final performance of edible coatings. It directly determines the fluidity, spread ability, film thickness, adhesion of the coating solution during the spraying process and the structural integrity formed after drying (Chen et al., 2009; Pereira et al., 2021). In the field of food packaging and preservation, changes in coating viscosity can affect the uniformity of its spread on the substrate and its curing behavior, thereby determining its moisture and gas barrier capabilities. Previous studies have pointed out that the flow behavior of coating solutions is significantly affected by factors such as polymer concentration, oil phase distribution, and emulsification stability (Kong et al., 2010).

In this study, eight GA-based formulations were systematically developed with constant total solids, while varying the ratios of the three components to investigate their influence on pre-spray viscosity. These viscosity measurements serve as a foundation for further analysis of film thickness, uniformity, and adhesion properties. The following Table S1 summarizes the pre-application viscosity values of each formulation.

Table S1 Viscosity measurements of pre-spray coating solutions formulated with varying ratios of GA, MPI, and CO (wt%)

Sample	Wt (%) (GA, MPI, CO)	Viscosity (mPa·s)
1	2, 4, 3	8.07
2	3, 4 ,2	9.99
3	3, 2, 4	7.05
4	4, 2, 4	7.35
5	4, 4, 2	5.67
6	5, 3, 2	10.71
7	5, 4, 1	13.83
8	6, 4, 2	10.68

The viscosity of the slurry directly affects the flow behavior of the coating during deposition and consequently determines the final film thickness. According to Schweizer (2022), in Newtonian fluid systems, the volumetric flow rate Q per unit width through a slit or nozzle is inversely proportional to the fluid viscosity under constant pressure and geometry. This principle implies that higher-viscosity slurries exhibit lower flow rates and therefore deposit more material per unit area, resulting in thicker coatings. The experimental data strongly support this theoretical prediction. For instance, Sample 7, which had the highest viscosity (13.83 mPa·s), yielded a visibly thicker film compared to low-viscosity samples such as

Sample 5 (5.67 mPa·s), which produced a much thinner layer. This trend can be attributed to the slower spreading and higher resistance to flow of more viscous slurries, which promotes material accumulation during the spraying process. Moreover, formulations with GA concentrations exceeding 4% showed a nonlinear increase in viscosity (Samples 6–8), which corresponded to a notable increase in film thickness due to enhanced gel-like structure formation in the slurry.

While high viscosity can increase film thickness, it may also compromise film uniformity. Viscosity inhomogeneity across the coating width (x-direction), caused by insufficient mixing or temperature gradients, can induce localized variations in Q(x), ultimately leading to non-uniform film thickness (Schweizer, 2022). For instance, Sample 7 (GA 5%, CO 1%, viscosity 13.83 mPa·s) likely experienced pronounced edge-to-center thickness differences during coating, consistent with Chae et al. (2020), who reported that high-viscosity solutions in spin-coating processes promote uneven fluid redistribution, resulting in thicker central regions and thinner boundaries (Fig. S2). Conversely, low-viscosity formulations such as Sample 5 (5.67 mPa·s) may achieve better uniformity but risk insufficient structural integrity due to reduced material cohesion (Kong et al.,2018; Zhang et al., 2016). These findings highlight the necessity of balancing viscosity within an optimal range to ensure both uniform deposition and mechanical robustness.

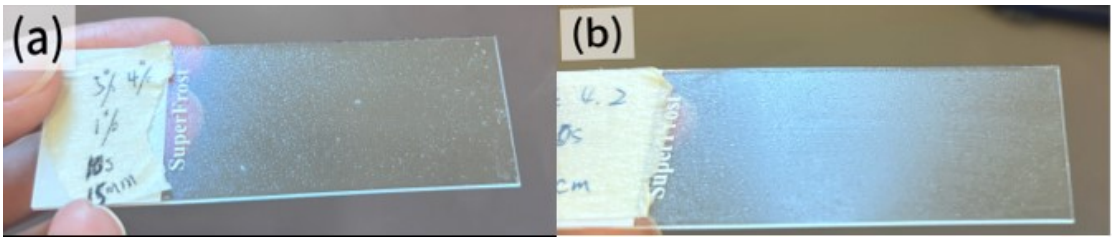

Fig. S2 Surface Morphology of Edible Coating Films Sprayed with Different Formulations: (a) 1-541: GA 5%, MPI 4%, CO 1% – Characterization of droplet distribution and coverage uniformity. (b) 1-442: GA 4%, MP 4%, CO 2% – Observation of film density and surface texture homogeneity.

What's more, the viscosity of the slurry is one of the key parameters influencing the adhesion and structural integrity of the coating. According to the liquid structure theory proposed by Grunberg and Nissan (1949), the energy of viscosity (E_visc) reflects the molecular interaction energy required to overcome cohesive forces during flow. When E_visc significantly exceeds the work of cohesion (W_c), it implies the presence of strong associative structures—such as hydrogen bonding or dipole–dipole interactions, which enhance both internal cohesion and adhesion to substrates. These associations improve the coating's resistance to mechanical stress and reduce peeling tendencies. In this study, high-viscosity formulations exhibited stronger adhesion and structural stability. Sample 7 formed a continuous, crack-free film with no signs of edge peeling, indicating effective bonding and cohesive integrity. In contrast, the low-viscosity Sample 5, though uniform, showed weak water resistance and poor anchoring, suggesting limited internal bonding. The binder composition explains this behavior: GA, rich in hydroxyl groups, contributes to viscosity through hydrogen bonding, while coconut oil reduces polarity and disrupts molecular interactions, thereby weakening both viscosity and

adhesion. Kong et al. (2018) and Zhang et al. (2016) have also shown that low-viscosity coatings tend to fail under thermal or mechanical stress due to insufficient internal cohesion. Tang et al. (2021) emphasized that when binder content is low, the "anchoring" and "interlocking" between particles diminish, resulting in poor adhesion. Therefore, maintaining a suitable viscosity is crucial for developing mechanically durable films. In our formulation system, a viscosity range of 9–11 mPa·s appeared optimal for balancing adhesion and film stability without introducing significant non-uniformity or flow resistance.

2.3 Transmittance measurement at 660 nm

The optical properties of edible coating solutions are vital in food packaging systems, particularly when visual clarity or transparency is a key consumer consideration. Transmittance not only reflects the compactness and uniformity of the coating structure but also indirectly indicates internal phase distribution and potential aggregation.

The variation of the mass ratio of different components will significantly affect the optical performance of the gel or coating system. For instance, a study based on the LMWG system found that by adjusting the proportion of different low-molecular-weight gel factors, the transmittance could be significantly improved, with the maximum value even approaching 96% (at 650 nm), while the single-component system exhibited extremely low light transmittance (Loos et al., 2021). This indicates that in the compound system, there may be a synergistic effect or structural reorganization among the components, forming a more stable or smooth network structure, thereby increasing the light transmittance.

Therefore, before conducting the spraying treatment, it is necessary to standardize the measurement of the light transmittance of different formulations (such as 660 nm wavelength) to provide reliable optical data support and offer a theoretical basis for the subsequent analysis of the uniformity, transparency and application adaptability of the coating.

According to the results (Fig. S3), the light transmittance of all samples is at an extremely low level (all below 26%), and the overall light transmittance is poor. Among them, the samples with the lowest light transmittance were 6,4,2 (10.5%), while the light transmittance of the samples with the highest light transmittance, 5,3,2, was 25.5%. High content of GA is closely related to increased absorbance, further inhibiting the transmission ability of light. Although the CO content in some formulations is relatively high (such as 3,2,4 or 4,2,4), which shows relatively high light transmittance to a certain extent, on the whole, the transmittance of the solutions in all formulations in the visible light region is insufficient to meet the application scenarios with high transparency requirements.

The poor light transmittance observed in high-GA formulations may be largely attributed to the optical behavior of gum Arabic itself. According to previous studies, GA molecules contain carboxyl groups and naturally occurring phenolic compounds that can absorb visible light, particularly near the 660 nm wavelength (Randall, 1992). In addition, GA can interact with proteins to form a more compact network, increasing turbidity. Furthermore, the higher viscosity promotes stronger molecular entanglement and enhances light scattering within the solution, making it more difficult for light to pass through.

However, formulation alone does not fully explain the low transparency. Physical processing parameters and structural properties of the coating also play a critical role in determining final light transmission. The spraying amount, heating temperature, structural density and thickness uniformity will all affect the optical properties of the film. According to the research of Skroznikova et al. (2013), under the conditions of moderate viscosity (3-5 mPa·s) and appropriate heat treatment (450°C), the light transmittance of the prepared SiO_2 coating can reach 92.12%. Moreover, the uniform and dense coating structure is conducive to reducing the scattering and absorption of light within the film, thereby enhancing the light transmittance. Pham et al., (2010) also reported that the light transmittance decreased with the increase of coating thickness. Among them, the light transmittance of the film layer formed by spraying the Go-Hydrazine dispersion at 240°C was approximately 84% at a wavelength of 550 nm. In addition, preheating the spraying at high temperatures can form a flatter surface, reduce light scattering and improve the overall optical performance.

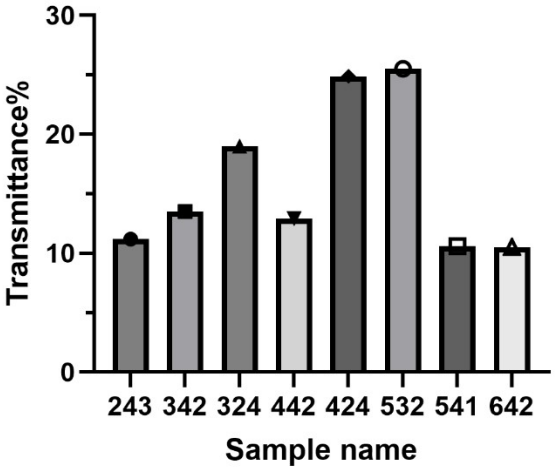

Fig. S3 Transmittance of Different Formulations Before Spraying: Each bar represents a specific coating formulation, labeled on the x-axis in the format (GA%, MPI%, CO%). The y-axis shows the corresponding light transmittance (%) measured before spraying. For example, "5, 3, 2" refers to a formulation containing 5 wt% GA, 3 wt% MP, and 2 wt% CO.

2.4 Visual Comparison of Film Surface Quality

A visual assessment of the spray-coated films from six GE-based formulations reveals notable differences in surface uniformity, transparency, and visual defects, which align with the previously measured physicochemical and microstructural properties.

The GE-based formulations were listed in Table S2 below. Among all samples, Formulations S6 and S9 demonstrated the most favorable visual characteristics, exhibiting smooth, continuous, and homogeneous surfaces with minimal observable imperfections. Specifically, S6 showed a uniformly glossy finish and minimal surface granularity, indicating excellent

emulsion stability and film-forming integrity. Similarly, S9 exhibited high transparency and consistent distribution, with only minor heterogeneity at the edges. These results suggest that the balanced composition of gelatin, MPI, and coconut oil in these formulations enabled stable droplet dispersion and efficient film coverage during spray application, likely due to optimal viscosity and surface interaction.

Table S2 Composition of edible film-forming solutions

S.NO	Gelatin (g/100 mL)	Coconut Oil (g/100 mL)	MPI (g/100 mL)
S6	4.0	4.0	4.0
S7	5.0	2.0	2.0
S8	4.0	2.0	4.0
S9	4.0	4.0	2.0
S10	4.0	2.0	2.0
S11	2.0	4.0	2.0

In contrast, Formulation S11—characterized by low gelatin and MPI content—presented a visibly less cohesive appearance. The film showed signs of unevenness and patchiness, with increased light scattering and dullness, possibly resulting from poor emulsification and phase separation. The low protein concentration may have failed to support an adequate network structure, leading to irregular droplet fusion and microvoid formation during drying. Formulation S8, though containing a relatively high amount of MPI, exhibited streaking and some visible disruptions along the film surface, suggesting localized drying heterogeneity or insufficient crosslinking during heat treatment. The imbalance between high MPI and lower oil content may have led to inconsistent migration or interfacial instability. Formulations S10 and S7 both displayed more noticeable roughness and non-uniformity. In particular, S10 had visible aggregation patterns and micro-patches, indicating potential droplet coalescence or interfacial breakdown. S7, though more visually consistent than S11 or S10, still lacked the clarity and gloss observed in S6 and S9, suggesting a moderately compact but less optimal matrix. These visual differences provide macroscopic evidence supporting microstructural observations and physicochemical measurements discussed in the study. They reinforce the conclusion that formulations S6 and S9 exhibited the best film-forming performance, offering promising potential for practical applications in spray-coated edible coatings.

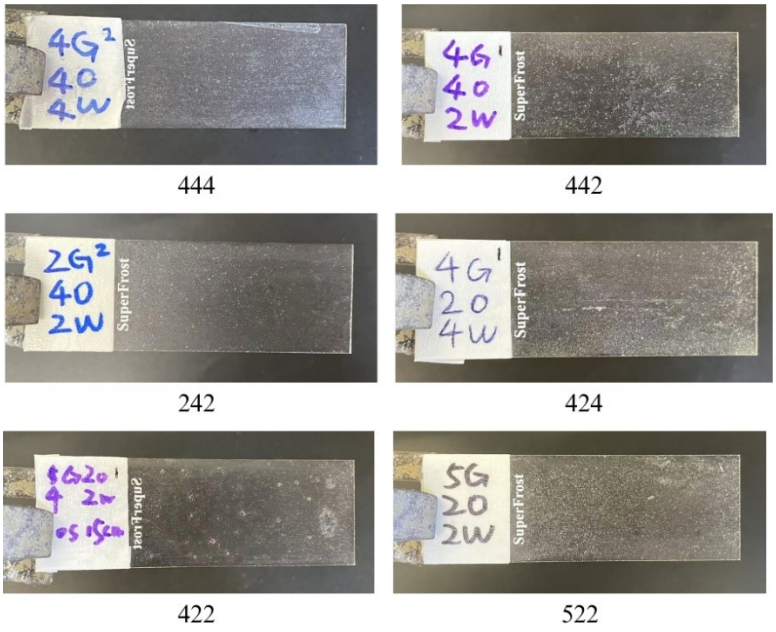

Fig. S4 Macroscopic Appearance of Spray-Coated Edible Films with Varying Gelatin–MPI–Coconut Oil Ratios (refer to Table S2 for formulation names)

2.5 Moisture content and water solubility

Compared to traditional casting, spray coating creates thin films more rapidly and minimizes material waste, offering significant advantages for industrial applications. However, spraying also presents challenges, such as difficulty in controlling film thickness and uniformity. Parameters like atomization pressure, spray distance, nozzle size, and solution viscosity can all affect the final coating quality. Excessively high spray pressure may lead to splashing or bouncing of the solution, while overly low pressure can result in uneven surfaces or insufficient coverage. Therefore, a handheld spray gun (Ozito X Power XChange, 18V lithium battery, Australia) was used in this study to apply the emulsions onto flat glass substrates (Menzel-Gläser microscope slides, 76 × 26 mm, pre-cleaned, Germany), aiming to explore the film-forming properties and surface uniformity of different formulations under standardized spray conditions. After drying, it was observed that the surface of the spray-coated films appeared relatively smooth and continuous. Samples S6 and S8 exhibited the most homogeneous surfaces with minimal defects. In contrast, samples S11 and S7 showed evident shrinkage and wrinkling, which may be related to emulsion instability or poor matrix connectivity during drying. The presence of pinholes and radial cracks in some samples suggests insufficient flexibility or uneven stress distribution during solvent evaporation. According to the literature, poor emulsification or phase separation can lead to uneven drying rates, causing local shrinkage or surface deformation (Liu et al., 2019).

Additionally, the initial droplet size of the emulsion and the strength of the interfacial film are critical factors influencing the final morphology. Smaller and more stable oil droplets tend to maintain their shape during drying, forming a smooth continuous layer, while larger droplets or aggregated droplets can easily rupture or collapse during drying, leaving cavities or

disrupting the matrix continuity (Chen et al., 2021). Among the six formulations, S6 demonstrated the best film-forming properties, attributed to its balanced MPI-to-gelatin ratio, moderate oil content, and high emulsion stability. This combination effectively supported the formation of a uniform surface and a robust internal network.

Table S3 Comparative microstructural evaluation and functional inference of GA/GE-based edible coating formulations based on surface integrity and uniformity

Sample name	Major characteristics including surface integrity and continuity, uniformity, and inference of coating performance
1-243	● No obvious cracks ● No hierarchical structure ● Uneven particle distribution ● Observable surface elevation variation ● Non-uniformity
1-342	● No cracks or layer separation ● Moderate roughness, some concavities ● Slightly poor continuity as highly populated with aggregated clusters ● Imbalanced distribution ● A wide size distribution of particles ● Moderate heterogeneity ● Moderate integrity with localized ghosting interference ● Slightly compromised barrier with moderate film integrity
1-324	● No cracks observed ● Relatively smooth surface, with some aggregated particles form local uplifted or uneven areas ● No obvious stratification ● Good overall continuity ● Presence of moderately varied distribution with generally balanced particle dispersion ● Mild surface undulation without significant roughness ● Acceptable uniformity ● Moderate vapor/gas barrier property
1-424	● No obvious linear cracks or film layer fractures observed ● Continuous structure without breaks ● Moderate irregularity observed ● Coexistence of large aggregates and scattered fine particles ● Poor uniformity
1-442	● Presence of several fine visible linear cracks ● Relatively smooth overall surface and continuous texture ● Good overall consistency of coating ● Relatively uniform of the distribution and coverage of the coating ● Evenly dispersed particles across the surface with small clustering ● Moderate uniformity
1-532	● No penetrating linear fractures found ● Relatively smooth surface ● High structural continuity ● Complete surface coverage without exposed substrate ● Relatively consistent particle spacing with small clustering regions ● Uniform dispersion

1-541	● Absence of penetrating linear cracks ● Smooth topology ● Non-stratified single-phase film ● Well-maintained surface coherence ● Homogeneity of spatial particle distribution without noticeable clustering ● Consistency in particle size with minimal presence of oversized agglomerates ● Evenness of surface morphology ● Intact coating film structure
1-642	● Absence of evident cracks ● Severe particle clustering with partial network formation ● Disrupted film continuity due to extensive particle aggregation and interstitial voids ● Distribution heterogeneity with zones exhibiting denser accumulation of aggregated particles
2-224	● No obvious cracks ● Larger internal pores ● Collapsed structures ● Oil droplets with a wide particle size distribution (3 – 30 μm) ● Partial coalescence or adhesion observed ● Extensive droplet fusion and matrix disintegration
2-422	● No obvious cracks ● Smooth microcapsule surface ● Fine and evenly dispersed internal voids ● Relatively large oil droplets (50 – 100 μm)
2-442	● Presence of several fine visible linear cracks ● Good structural performance ● Larger internal pores ● Collapsed structures ● Poor uniformity
2-444	● Presence of several fine visible linear cracks ● Unsmooth surface ● Good droplet dispersion ● A little heterogeneity in microstructure ● Relatively uniform surface
2-424	● No obvious cracks ● Some collapsed structures ● Small oil droplets observed (5 – 20 μm) ● Relatively smooth surface
2-522	● No obvious cracks ● Moderate to small oil droplets (4 – 15 μm) observed ● Less compact background matrix ● Localized droplet aggregation ● Porous background with light granularity ● Relatively large dents were present

Table S4 Comparative visual and textural evaluation of 1-541 coated and uncoated banana samples during room temperature storage: A day-by-day sensory observation from initial state to advanced ripening and decay

Time	Sample group 1	Sample group 2	Control group
Day 0	The entire banana is light yellow in color, with intact and undamaged skin. There is a local greenish tinge on the stem and a distinct large black spot at the tail.	The entire banana is yellow, with some areas of greenness on the stem. The surface is relatively smooth, the texture is relatively uniform, and there is a distinct large black spot in the middle	The entire banana is yellow, with some areas of the stem turning green. The overall surface is smooth but without coating protection, and no obvious black spots are seen.
Day 1	The bananas have a uniform yellowish color, with the green color disappearing. The skin is slightly dry but without obvious spots or cracks. The coating is intact and adhered, and the shape remains good. No peeling or collapse is observed.	Some of the bananas in sample 2 have small black spots. There is one black patch, which is still green. The coating has not peeled off and adheres well, still maintaining its original curved state.	The epidermis turned significantly darker and was covered with brown spots. The local skin became soft and began to show slight sagging.
Day 2	Light-colored spots appeared locally. The overall degree of discoloration was relatively small, maintaining the original shape. The surface slightly lost water but no obvious rot was observed, and the performance was stable.	The cyan color has not completely disappeared, with small brown spots appearing in some areas. There are black spots on the ridges, and the stem is black.	The entire banana has small brown spots, more than yesterday. Two large blackboards have appeared at the tail, and the stem has turned black.
Day 3	The banana peel appears slightly yellowish, with localized brown spots slightly darker than Day 2. The area near the stem is mildly shriveled, but the overall coating remains intact.	The surface remains smoother than Group 1, but light brown speckles are now visible. with only mild browning near the stalk and no visible decay. The overall color is light yellow brown.	Obvious brown spots have appeared on the skin of the bananas. The part near the fruit stem is somewhat black. The color of the skin is more yellowish and brownish than that of the other two groups. They are more mature or have more severe oxidation.
Day 7	The overall color is slightly yellowish, with a clean surface. Only a few small brown spots appear, and the area near the fruit stem is slightly dried up. The coating is intact and ages	The skin of the banana is damaged. The color is slightly darker, with more spots than Sample 1, and striped, brown spots have appeared at the tail. The overall structure is complete with slight mature	The skin of bananas is dark yellow, with a dense increase of brownish spots, especially concentrated in the middle and later sections. The fruit stem area is slightly soft, showing obvious signs of

	slowly.	changes.	aging but not yet collapsed.
Day 8	The epidermis color tends to be yellowish-brown, with a few fine brown spots scattered. It remains smooth and structurally intact near the fruit stalk, and the ripening is delayed.	The brown spots increased, were more widely distributed, the fruit stalks and tails slightly darkened, the epidermis slightly lost water, and the aging trend was obvious, but it was still better than the control.	The range of brown spots further expands, with some turning into black spots. The epidermis slightly collapses, especially near the tail area, and the fruit feels soft to the touch.
Day 9	There are small areas of deep brown spots. The overall structure remains tight. There is no sign of spoilage, and it is in a naturally mature and soft state. It is the best-preserved sample.	Dark patches appeared at the tail, and both ends. The peel was clearly ripe, slightly soft but not rotten. It is closer to the fully mature state than Sample 1.	The bananas have turned black over a large area, with loose and collapsed peels. Rotten water stains have appeared near the fruit stems, and the whole plant has entered a rapid stage of spoilage.
Day 10	Compared with the ninth day, the epidermal color of Sample 1 was slightly darker, the number of brown spots slightly increased, the distribution was still relatively uniform, the overall epidermis was still tight and without collapse, and the preservation state was better than that of other samples, showing a strong effect of delaying ripening.	It has become even darker compared to the ninth day, with the area of the black spots expanding, especially in the tail and middle regions. The fruit peel lost water significantly, the surface texture became soft, and there was a clear tendency to ripen and rot, but it was still better than control.	The color changes from deep yellowish-brown to blackish brown, with black spots distributed in contiguous areas. The epidermis collapses more obviously, and the fruit stalks dehydrate and curl, showing signs of spoilage. Compared with the ninth day, the degree of degradation has increased sharply.

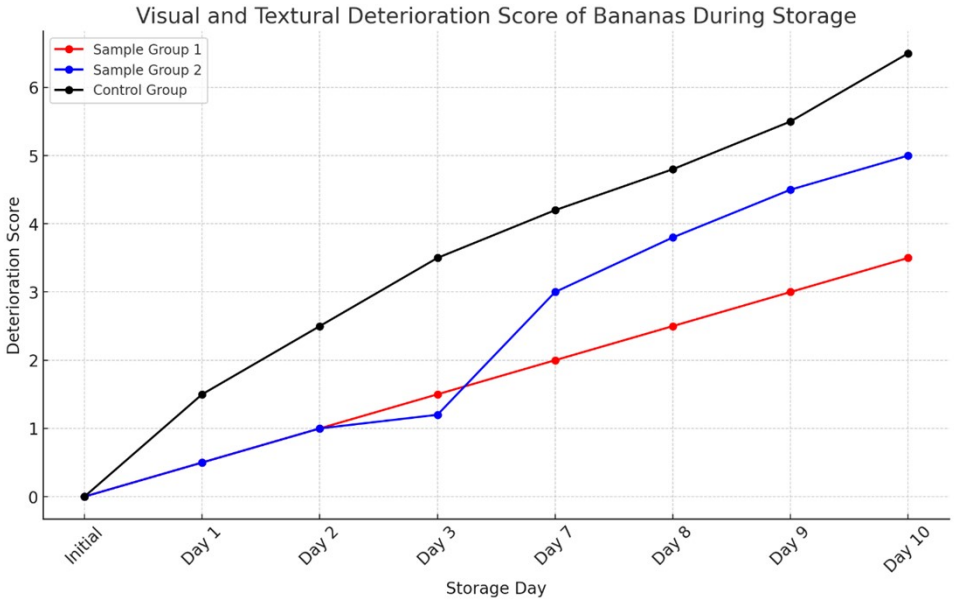

Fig. S5 Comparative evolution of visual and textural deterioration scores in coated and uncoated banana samples during 10-Day ambient storage: Evaluating the preservation effect of GA/MP/CO-based edible coating formulations (score based on Table S4)

References

Cai, Z., Deng, S., Liao, H., Zeng, C., & Montavon, G. (2014). The effect of spray distance and scanning step on the coating thickness uniformity in cold spray process. *Journal of thermal spray technology*, *23*, 354-362.

Debeaufort, F., Quezada-Gallo, J. A., & Voilley, A. (1998). Edible films and coatings: tomorrow's packagings: a review. *Critical Reviews in food science*, *38*(4), 299-313.

Erben, M., Pérez, A. A., Osella, C. A., Alvarez, V. A., & Santiago, L. G. (2019). Impact of gum arabic and sodium alginate and their interactions with whey protein aggregates on bio-based films characteristics. *International Journal of Biological Macromolecules*, *125*, 999-1007.

Guo, D., Kazasidis, M., Hawkins, A., Fan, N., Leclerc, Z., MacDonald, D., ... & Jodoin, B. (2022). Cold spray: over 30 years of development toward a hot future. *Journal of thermal spray technology*, *31*(4), 866-907.

Kamper, S. L., & Fennema, O. (1984). Water vapor permeability of an edible, fatty acid, bilayer film. Journal of Food Science, 49(6), 1482–1485. https://doi.org/10.1111/j.1365-2621.1984.tb12826.x

Kang, S., Bai, Q., Qin, Y., Liang, Q., Hu, Y., Li, S., & Luan, G. (2024). Film-forming modifications and mechanistic studies of soybean protein isolate by glycerol plasticization and thermal denaturation: A molecular interaction perspective. *Food Research International*, *196*, 115042.

Kong, M., Chen, X. G., Xing, K., & Park, H. J. (2010). Antimicrobial properties of chitosan and mode of action: a state of the art review. *International journal of food microbiology*, *144*(1), 51-63.

Krochta, J. M. (2002). Proteins as raw materials for films and coatings: definitions, current status, and opportunities. *Protein-based films and coatings*, *1*, 1-40.

Liu, T. P. (1982). Nonlinear stability and instability of transonic flows through a nozzle. *Communications in Mathematical Physics*, *83*, 243-260.

Loos, J. N., Boott, C. E., Hayward, D. W., Hum, G., & MacLachlan, M. J. (2021). Exploring the tunable optical and mechanical properties of multicomponent low-molecular-weight gelators. *Langmuir*, *37*(1), 105-114.

Maqbool, M., Ali, A., Alderson, P. G., Mohamed, M. T. M., Siddiqui, Y., & Zahid, N. (2011). Postharvest application of gum arabic and essential oils for controlling anthracnose and

quality of banana and papaya during cold storage. *Postharvest biology and technology*, *62*(1), 71-76.

Morillon, V., Debeaufort, F., Blond, G., Capelle, M., & Voilley, A. (2002). Factors Affecting the Moisture Permeability of Lipid-Based Edible Films: A Review. *Critical Reviews in Food Science and Nutrition*, *42*(1), 67–89. https://doi.org/10.1080/10408690290825466

Nath, A., Deka, B. C., Singh, A., Patel, R. K., Paul, D., Misra, L. K., & Ojha, H. (2012). Extension of shelf life of pear fruits using different packaging materials. Journal of food science and technology, 49, 556-563.

Nitbani, F. O., Tjitda, P. J. P., Nitti, F., Jumina, J., & Detha, A. I. R. (2022). Antimicrobial properties of lauric acid and monolaurin in virgin coconut oil: a review. *ChemBioEng Reviews*, *9*(5), 442-461.

Nunes, C. N., & Emond, J. P. (2007, December). Relationship between weight loss and visual quality of fruits and vegetables. In *Proceedings of the Florida state Horticultural society* (Vol. 120, pp. 235-245).

Paul, S. K., Sarkar, S., Sethi, L. N., & Ghosh, S. K. (2018). Development of chitosan based optimized edible coating for tomato (Solanum lycopersicum) and its characterization. *Journal of food science and* technology, 55, 2446-2456.

Pereira, G. V. D. S., Pereira, G. V. D. S., Oliveira, L. C. D., Cardoso, D. N. P., Calado, V., & Lourenço, L. D. F. H. (2021). Rheological characterization and influence of different biodegradable and edible coatings on postharvest quality of guava. *Journal of Food*

Randall, R. C. (1992). *Molecular characterisation and functional properties of gum arabic*. University of Salford (United Kingdom).

Ren, J., Sun, Y., Hui, J., Ahmad, R., & Ma, Y. (2023). Coating thickness optimization for a robotized thermal spray system. *Robotics and Computer-Integrated Manufacturing*, *83*, 102569.

Romanazzi, G. (2010). Chitosan treatment for the control of postharvest decay of table grapes, strawberries and sweet cherries. Fresh Produce, 4(1), 111-5.

Schweizer, P. M. (2022). Film thickness and film thickness uniformity. In *Premetered Coating Methods: Attractiveness and Limitations* (pp. 387-452). Cham: Springer International Publishing.

Shao, H., Chen, Z., Chang, J., Yin, X., Chen, Y., Liu, Y., ... & Yang, W. (2024). Gum Arabic microgel–based biomimetic waterborne anticorrosive coatings with reinforced water and abrasive resistances. *Carbohydrate Polymers*, *342*, 122408.

Singh, H., Sidhu, T. S., Kalsi, S. B. S., & Karthikeyan, J. (2013). Development of cold spray from innovation to emerging future coating technology. *Journal of the Brazilian Society of Mechanical Sciences and Engineering*, *35*(3), 231-245.

Valencia-Chamorro, S. A., Palou, L., Del Río, M. A., & Pérez-Gago, M. B. (2011). Antimicrobial edible films and coatings for fresh and minimally processed fruits and vegetables: a review. *Critical reviews in food science and nutrition*, *51*(9), 872-900.

Xiao, M., Luo, L., Tang, B., Qin, J., Wu, K., & Jiang, F. (2022). Physical, structural, and water barrier properties of emulsified blend film based on konjac glucomannan/agar/gum Arabic incorporating virgin coconut oil. *Lwt*, *154*, 112683.

Zhang, Y., Zhang, S., & Wu, S. (2019). Room-temperature fabrication of TiO2-PHEA nanocomposite coating with high transmittance and durable superhydrophilicity. *Chemical Engineering Journal*, *371*, 609-617.